J. Fluid Mech. (1989), *vol.* 201, *pp.* 35–56
Printed in Great Britain

Deflection of a two-dimensional natural convection wake due to the presence of a vertical surface in close proximity

By RAVINDRA AGARWAL AND YOGESH JALURIA
Department of Mechanical and Aerospace Engineering, Rutgers University, New Brunswick, NJ 08903, USA

(Received 21 April 1986 and in revised form 17 August 1988)

The interaction between a freely rising thermal plume and an unheated vertical surface in its neighbourhood has been investigated. The underlying transport mechanisms are of interest from a fundamental standpoint, as well as in a variety of practical problems, such as the cooling of electronic equipment and room fires. A detailed numerical and experimental study of the flow is carried out. The temperature and velocity gradients are expected to be large, particularly near the thermal source. Also, any constraints imposed on the entrainment into the flow in the vicinity of the source are expected to significantly affect the nature of the flow and the interaction. These considerations make it imperative to solve the full governing equations in the interaction region. These equations are solved numerically by finite-difference methods, employing the vorticity–stream function formulation. The important physical variables in the problem are the total thermal energy input by the source, the size of the source, and the distance of the source from the vertical wall which is taken as adiabatic or isothermal in the computation. The flow is found to be strongly deflected towards the vertical surface for the parametric ranges considered. As expected, the diffusion effects in the main flow direction are found to decay downstream and the flow to gradually approach the characteristics of a wall plume resulting from a concentrated line heat source with the same total heat input. Thus, the axial diffusion terms may be neglected far downstream, allowing the flow there to be approximated as a boundary layer, with the full equations being solved in the interaction region. Finally, an experimental investigation is carried out to characterize the nature of the interaction. The flow is visualized by means of a shadowgraph and the temperature field is measured in the interaction region, downstream of the source. Numerical predictions agree with the experimental results, lending support to the numerical model for this interaction.

1. Introduction

Natural convection wakes generated by isolated thermal sources located in extensive ambient media occur very frequently in many technological applications and in the environment. However, in many circumstances, these wakes occur near each other or near solid boundaries. The nature of their interation with a surface or with one other and the effect of such an interaction on thermal transport are important from a fundamental as well as a practical viewpoint, see Gebhart *et al.* (1988). A relevant example is the cooling of electronic equipment by natural convection. In the absence of an externally induced flow, an electronic component dissipates the input electrical energy as heat and gives rise to a buoyancy-driven flow

that rises above the energy source as a wake or a plume. The interaction of this plume with unheated surfaces and with flows arising from other thermal sources in the neighbourhood is an important consideration in the positioning of these components, since the heat transfer characteristics are strongly affected by this interaction (Jaluria 1985*a*). Other examples include the flow due to a room fire or the natural convection flow in a cavity with localized heating, such as that due to solar energy input. In the case of enclosure fires, the heating of the wall and the spread of combustion products are substantially affected by such an interaction between the fire plume and the adjacent wall, see Quintiere (1984).

Early studies of the interaction of free boundary flows with neighbouring surfaces and with other flows considered non-buoyant jets. See, for example, the papers by Bourques & Newman (1960), Miller & Comings (1960), and Sawyer (1963). The flow resulting from the interaction of thermal plumes rising from an array of heated elements was studied experimentally by Lieberman & Gebhart (1969). Some work has also been done on laminar plume interactions, see Gebhart *et al.* (1988). Experimental investigations have been carried out in several of these studies, largely by flow visualization, followed by analytical predictions of the interaction on the basis of simple approximations of the induced entrainment. See the work for Pera & Gebhart (1975) and Gebhart, Shaukatullah & Pera (1976). Jaluria (1982) carried out an experimental study of the interaction of a laminar two-dimensional thermal plume, arising from a concentrated, line, heat source, with a neighbouring vertical surface.

In all these investigations, the basic mechanism of the interaction has been shown to be the restriction imposed on the fluid entrained downstream by the plume, due to the presence of the neighbouring surfaces or other flows. This is the natural convection equivalent of the Coanda effect, see Reba (1966). The demand for entrainment results in a pressure difference which causes the ambient fluid to be drawn into the plume. A neighbouring surface curtails this entrainment and, thus, causes a pressure imbalance which forces the plume toward the surface. The resulting interaction has, therefore, been found to be quite sensitive to the geometry of the flow configuration. However, there has been no detailed analytical or numerical investigation of the flow field and of associated pressure imbalance in such plume interactions. Of particular interest here is the numerical simulation of these flows to determine the effect of entrainment curtailment on the pressure field and on the flow.

The present study considers the interaction of a two-dimensional natural convection wake arising from a long, finite-size heat source with a neighbouring unheated vertical surface. The source is positioned close to the vertical surface, at a distance varying from zero to a few source widths. A configuration considered in detail assumes the thermal source to be located on an unheated, adiabatic or isothermal, horizontal surface at the leading edge of the vertical surface, as shown in figure 1. A uniform surface heat flux input, over the source width, is imparted by the thermal source. The vertical and horizontal surfaces are considered as isothermal or adiabatic in the analysis, with the experimental study approximating the latter condition. Other geometries and boundary conditions are also considered in this study, as discussed later in the paper.

The temperature and velocity gradients in the flow are relatively large, in both the vertical and horizontal directions, giving rise to strong diffusion effects in both directions. This makes the problem elliptic in nature, since the terms representing diffusion in the main flow direction may not be neglected in the governing equations.

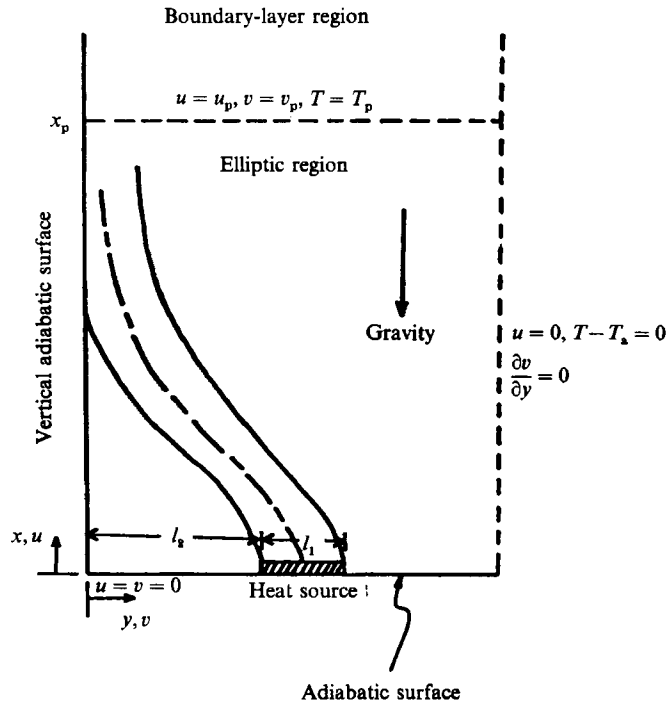

FIGURE 1. One of the flow configurations considered and the corresponding coordinate system, with the relevant boundary conditions.

Therefore, boundary-layer assumptions cannot be employed and the full energy and Navier–Stokes equations have to be solved, particularly near the thermal source. These equations are solved, numerically, by finite-difference methods. The downstream boundary conditions are obtained by neglecting the vertical diffusion terms far downstream and solving the resulting boundary-layer equations in this region, as discussed in detail in the paper. Because of the basic characteristics of the flow, outlined above, the boundary conditions that influence the fluid entrainment into the flow are expected to strongly affect the interaction. Different boundary conditions were considered here and it was confirmed that they do indeed affect the flow substantially.

Of particular interest in this work are the nature of the interaction, the temperature and velocity profiles in the flow, and the characteristics of the wall plume flow far downstream of the heat source. These considerations are related to a basic understanding of this flow circumstance and to the relevant heat removal process from, for example, finite-size electronic components on a circuit board. The important physical parameters in this problem are the distance of the heat source from the vertical wall l_2, and the heat flux input q at the source surface. The Grashof number Gr, which is based on the width of the heat source l_1 and the surface heat flux, and the ratio l_2/l_1 arise as important dimensionless parameters. The Prandtl number Pr is taken as 0.7, which applies for air at room temperature, the flow is assumed to be two-dimensional in the numerical study and the height of the source is taken as negligible compared to its width.

An experimental investigation was also carried out in order to verify the numerical predictions. The flow was visualized by means of a shadowgraph and the temperature

field was measured by means of thermocouples in the interaction region and in the flow adjacent to the wall, downstream of the source.

The numerical results were found to be in general agreement with earlier studies on similar flows. For the range of the physical variables considered, the interaction was found to be very strong, as seen from the deflection toward the surface. This is presented quantitatively in terms of the flow trajectory and the location where the flow meets the surface. The flow geometry was found to be a dominant aspect in such an interaction, since it affects the restriction, if any, on the ambient-fluid entrainment into the flow. The interaction was found to grow stronger with increasing total heat input and to weaken as the source was moved away from the wall, as expected. The temperature profiles measured experimentally showed trends that were quite similar to those predicted numerically. The pressure difference across the flow was also computed and the results indicate quantitatively the imbalance due to the restriction imposed on the entrainment. The numerical simulation of such interacting flows is discussed in terms of the important considerations that arise, particularly with respect to entrainment into the flow. Several other interesting features related to the basic nature of the flow interaction were observed in this work.

2. Analysis and numerical scheme

The flow under consideration is shown in figure 1 for a particular geometry, along with the coordinate system employed. A heat source of negligible height and width l_1 is positioned at a distance l_2 from a vertical adiabatic surface. The source has a uniform heat flux input q at the surface. The third direction is taken as large so that a two-dimensional flow may be assumed. The source is assumed to be located on a horizontal, adiabatic or isothermal, surface at the level of the leading edge of an adiabatic or isothermal vertical plate. Other boundary conditions, such as the one that arises when the horizontal bottom plate is absent, were also considered.

2.1. *Governing equations*

The full governing equations, in the Cartesian coordinate system, for the natural convection flow shown in figure 1 may be written for a laminar, steady, two-dimensional flow, employing the Boussinesq approximations for the density variation, assuming the remaining properties to be constant and neglecting viscous dissipation and pressure work effects, as (Jaluria 1980)

$$\frac{\partial u}{\partial x}+\frac{\partial v}{\partial y}=0, \tag{1}$$

$$u\frac{\partial u}{\partial x}+v\frac{\partial u}{\partial y}=-\frac{1}{\rho}\frac{\partial p}{\partial x}+\nu\left(\frac{\partial^2 u}{\partial x^2}+\frac{\partial^2 u}{\partial y^2}\right)+g\beta(T-T_a), \tag{2}$$

$$u\frac{\partial v}{\partial x}+v\frac{\partial v}{\partial y}=-\frac{1}{\rho}\frac{\partial p}{\partial y}+\nu\left(\frac{\partial^2 v}{\partial x^2}+\frac{\partial^2 v}{\partial y^2}\right), \tag{3}$$

$$u\frac{\partial T}{\partial x}+v\frac{\partial T}{\partial y}=\alpha\left(\frac{\partial^2 T}{\partial x^2}+\frac{\partial^2 T}{\partial y^2}\right), \tag{4}$$

where x and y are the coordinate distances, shown in figure 1, and u and v are the vertical and horizontal velocity components, respectively. The local pressure and temperatures are denoted by p and T, respectively, T_a is the ambient temperature,

and g is the magnitude of the acceleration due to gravity. Also, ρ, ν, α, and β denote the density, kinematic viscosity, thermal diffusivity and the coefficient of thermal expansion of the fluid, respectively.

The vertical diffusion terms in the above equations are expected to become negligible, compared to the transverse diffusion terms, far downstream. Thus, the flow far from the interaction region may be approximated as a boundary-layer flow governed by the equations

$$\frac{\partial u}{\partial x}+\frac{\partial v}{\partial y}=0, \tag{5}$$

$$u\frac{\partial u}{\partial x}+v\frac{\partial u}{\partial y}=\nu\frac{\partial^2 u}{\partial y^2}+g\beta(T-T_a), \tag{6}$$

$$u\frac{\partial T}{\partial x}+v\frac{\partial T}{\partial y}=\alpha\frac{\partial^2 T}{\partial y^2}. \tag{7}$$

This implies that the flow region far downstream may be considered in terms of the usual boundary-layer approximations, with the interaction region being governed by the full, elliptic equations. This treatment has been considered in detail by Jaluria (1985*b*) who has also shown that the leading-edge effects decay downstream and that the flow approaches the characteristics of a wall plume generated by a concentrated line source with the same total energy input as the given source. Jaluria & Gebhart (1977) studied such wall plumes using similarity methods. Of course, in practice, the flow may undergo transition to turbulence downstream. A suitable closure model would then be needed to simulate the turbulent wall plume thus generated, see Grella & Faeth (1975). These considerations are discussed further in terms of the boundary conditions and the numerical scheme, in the next two subsections.

2.2. *Boundary conditions*

The boundary conditions for the full equations, (1)–(4), can be obtained from the ambient conditions, from the no-slip and thermal conditions at the wall, and from the characteristics of the boundary-layer wall plume that arises far downstream. Thus, for adiabatic vertical and horizontal surfaces in figure 1,

$$\text{at } y=0, \quad x>0; \quad u=0, \quad v=0, \quad \frac{\partial T}{\partial y}=0, \tag{8a}$$

$$\text{as } y\to\infty, \quad x>0; \quad u\to 0, \quad \frac{\partial v}{\partial y}\to 0, \quad T-T_a\to 0, \tag{8b}$$

$$\text{at } x=0; \quad u=0, \quad v=0 \quad \text{for} \quad y>0 \tag{9a}$$

and

$$q=-k\frac{\partial T}{\partial x} \quad \text{for} \quad l_2\leqslant y\leqslant (l_1+l_2),$$

$$\frac{\partial T}{\partial x}=0 \quad \text{for} \quad 0<y<l_2 \quad \text{and} \quad y>(l_1+l_2). \tag{9b}$$

The gradient condition on v in (8*b*), instead of $v\to 0$, is more appropriate for a numerical solution, since it is a weaker condition than the latter and allows a more gradual adjustment to the ambient conditions, see Chan & Tien (1985). This condition results in the requirement of a smaller computational domain than if

$v \to 0$ were used instead, see Jaluria & Torrance (1986). Thus, the gradient condition reduces the computational effect while maintaining the desired accuracy level.

The boundary conditions at a downstream location x_p beyond which the flow is treated as a boundary-layer flow, governed by (5)–(7) are specified as

$$\text{at } x = x_p; \quad u = u_p, \quad v = v_p, \quad T = T_p, \tag{10}$$

where the subscript p refers to the solution of the parabaolic, boundary-layer equations. The variables u, v and T are to be obtained numerically, as discussed later. Here, x_p is varied till the numerical results become independent of the chosen value. The vertical diffusion terms must become negligible by this distance, as also confirmed from the numerical results for the elliptic region.

In the absence of the horizontal surface, with the vertical plate extending to infinity downward, the boundary conditions for the region below the source at $x = 0$ are obtained as

$$\text{at } y = 0, \quad x < 0; \quad u = 0, \quad v = 0, \quad \frac{\partial T}{\partial y} = 0, \tag{11}$$

$$\text{at } x \to -\infty, \quad y > 0; \quad \frac{\partial u}{\partial x} \to 0, \quad v \to 0, \quad T - T_a \to 0. \tag{12}$$

Thus, these boundary conditions allow the ambient entraining fluid to enter the computational domain with zero shear at the boundaries. Similarly, boundary conditions may be written for other flow configurations.

To facilitate the numerical solution of these equations, (1)–(4) were rewritten in the conservative and unsteady form, in terms of the vorticity and the stream function, as discussed in detail by Roache (1976) and Jaluria & Torrance (1986). The equations were non-dimensionalized with l_1 and q as characteristic quantities, leading to the dimensionless variables

$$X = x/l_1, \quad Y = y/l_1, \quad U = u/U_c, \quad V = v/U_c, \tag{13a}$$

$$\Omega = \omega/(U_c/l_1), \quad \Psi = \psi/(U_c l_1), \tag{13b}$$

$$\theta = (T - T_a)/(ql_1/k), \quad \tau = \tau'/(l_1/U_c). \tag{13c}$$

Also,

$$U_c = \left(\frac{g\beta q l_1^2}{k}\right)^{\frac{1}{2}}, \quad Gr = \frac{g\beta q l_1^4}{k\nu^2}, \quad Pr = \frac{\nu}{\alpha}, \tag{13d}$$

$$\omega = \frac{\partial v}{\partial x} - \frac{\partial u}{\partial y}, \quad u = \frac{\partial \psi}{\partial y}, \quad v = -\frac{\partial \psi}{\partial x}. \tag{13e}$$

Here ω is the physical vorticity, ψ the physical stream function, τ' the physical time, U_c the convection velocity, Pr the Prandtl number, and Gr the Grashof number based on ql_1/k as the characteristic temperature difference. The total heat input Q, per unit transverse dimension of the source, is therefore ql_1. This non-dimensionalization is frequently employed for natural convection flows generated by uniform heat flux surfaces (Gebhart *et al.* 1988).

The vorticity–stream function formulation is obtained by taking the y-derivative of (2) and the x-derivative of (3) and subtracting the former from the latter to

eliminate the pressure term, i.e. taking the curl of the vector momentum equation. The resulting non-dimensional equations are

$$\frac{\partial \Omega}{\partial \tau}+\frac{\partial}{\partial X}(U\Omega)+\frac{\partial}{\partial Y}(V\Omega)=\frac{1}{Gr^{\frac{1}{2}}}\left(\frac{\partial^2\Omega}{\partial X^2}+\frac{\partial^2\Omega}{\partial Y^2}\right)-\frac{\partial \theta}{\partial Y}, \tag{14}$$

$$\frac{\partial^2 \Psi}{\partial X^2}+\frac{\partial^2 \Psi}{\partial Y^2}=-\Omega, \tag{15}$$

$$\frac{\partial \theta}{\partial \tau}+\frac{\partial}{\partial X}(U\theta)+\frac{\partial}{\partial Y}(V\theta)=\frac{1}{Pr\,Gr^{\frac{1}{2}}}\left(\frac{\partial^2\theta}{\partial X^2}+\frac{\partial^2\theta}{\partial Y^2}\right), \tag{16}$$

where the continuity equation has also been employed to put the equations in conservative form, i.e. with $V\cdot\nabla\phi$ replaced by $\nabla\cdot(V\phi)$ where V is the velocity vector and ϕ represents the convected quantity Ω or θ. See Jaluria & Torrance (1986) for details. Similarly, the boundary conditions can be obtained in terms of the dimensionless quantities, using (13). For instance, in the ambient medium as $Y\to\infty$, $\partial\Omega/\partial Y\to 0$, $\theta\to 0$ and $\partial\Psi/\partial Y\to 0$. At the two surfaces in figure 1, Ψ is taken as zero. The wall vorticity is obtained by using the definition of Ω in (13) and Taylor series, see Jaluria & Torrance (1986). Matching of the velocity components and the temperature, obtained from the calculations for the two regions shown in figure 1, is done at the interface $X=X_p$, whose location is varied to ensure that the numerical results are independent of the value chosen.

The unsteady boundary-layer equations that apply far downstream, in the parabolic region, are obtained, using the non-dimensionalization given in (13), as

$$\frac{\partial U}{\partial X}+\frac{\partial V}{\partial Y}=0, \tag{17}$$

$$\frac{\partial U}{\partial \tau}+U\frac{\partial U}{\partial X}+V\frac{\partial U}{\partial Y}=\frac{1}{Gr^{\frac{1}{2}}}\frac{\partial^2 U}{\partial Y^2}+\theta, \tag{18}$$

$$\frac{\partial \theta}{\partial \tau}+U\frac{\partial \theta}{\partial X}+V\frac{\partial \theta}{\partial Y}=\frac{1}{Pr\,Gr^{\frac{1}{2}}}\frac{\partial^2\theta}{\partial Y^2}. \tag{19}$$

The boundary conditions for these equations are

$$\text{at } Y=0,\quad X>X_p;\quad U=0,\quad V=0,\quad \frac{\partial\theta}{\partial Y}=0, \tag{20a}$$

$$\text{as } Y\to\infty,\quad X>X_p;\quad U\to 0,\quad \theta\to 0. \tag{20b}$$

2.3. *Numerical scheme*

The boundary conditions at $X=X_p$ are obtained by the simultaneous solution of the equations for the elliptic and the boundary-layer regions. Starting with an initial no-flow condition, the conditions at X_p are allowed to develop with time. Thus, the full equations are solved in the elliptic region and the boundary-layer equations in the parabolic region, using the computed velocity and temperature at the interface from the previous time-step. As mentioned above, the location of the interface X_p is moved downstream till the numerical results are found to become essentially unchanged by a further increase in X_p. For the conditions considered in this paper, an X_p of around 5.0 was found to be quite satisfactory. The details of the numerical procedure are given by Jaluria & Agarwal (1986).

The given problem can be solved as an elliptic problem, governed by the full Navier–Stokes equations, over the entire flow region, rather than breaking it into two regions, as shown in figure 1. However, the vertical diffusion terms are expected to decay downstream, allowing the flow far downstream to be treated as a boundary layer, see Yang & Jerger (1984). This simplifies the computation very substantially, since the solution of the full elliptic equations is much more involved and time-consuming than that of the boundary-layer equations. Also, by eliminating the vertical diffusion terms downstream, the interaction becomes independent of the conditions far downstream in the parabolic region, as is physically expected. The parabolic region may easily be extended as far downstream as desired in order to study the characteristics of the wake far from the interaction region. For further details on these aspects, see Hardwick & Levy (1973) and Jaluria (1985*b*).

The full equations, (14)–(16), were solved numerically by employing finite-difference methods. The false transient method of Mallinson & de Vahl Davis (1975) was used to accelerate convergence to steady-state conditions. The Alternating Direction Implicit (ADI) scheme of Peaceman & Rachford (1955), with second-order upwind differencing for the convection terms and central differencing for the diffusion terms was used for solving the unsteady state equations. For the parabaolic region, the boundary-layer equations, (17)–(19), were solved by a finite-difference approach, employing time marching and an implicit formulation. The solution provided the boundary conditions at $X = X_p$ for the full equations. The initial condition was taken as zero flow and the convergence of the solution to the steady state at large time was determined. The grid spacing, the convergence criterion for the termination of the computation at steady state, the location of the interface X_p, and the initial conditions were varied so as to ensure that the effect of the chosen values on the converged steady-state results was negligible.

3. Experimental arrangement

The interaction of a two-dimensional thermal plume with a vertical surface was studied experimentally by Pera & Gebhart (1975) and by Jaluria (1982). In these studies, the plume was generated by the electrical heating of a fine metal wire. The present study is carried out with heat sources of finite width. Such sources are of particular interest in many practical problems such as those related to enclosure fires and electronic circuitry. However, no work has so far been done on finite-size sources. For this reason, an experimental investigation was also carried out, in conjunction with the numerical effort, in order to study the nature of the interaction and of the resulting flow, and also to compare the numerical and experimental results. The temperature distributions at the surface and in the flow, downstream of the thermal source, were measured, indicating the basic characteristics of the interaction and of the resulting thermal field. However, the experimental work was not as extensive as the numerical effort and was largely undertaken to provide support for the latter. Flow visualization was employed to observe the resulting flow.

A schematic of the experimental arrangement is shown in figure 2. A thin stainless steel strip of thickness 2.54×10^{-5} m and of width l_1 was used as a heat source to generate the natural convection wake, as shown. The strip was mounted on sliding clamps so that it would be positioned at a desired distance l_2 from the vertical surface, with l_2/l_1 ranging up to about 15. However, for a strong interaction l_2/l_1 was generally kept less than 5. At larger values, the interaction was found to be negligible, as expected, and the wake rose vertically. A d.c. power supply was

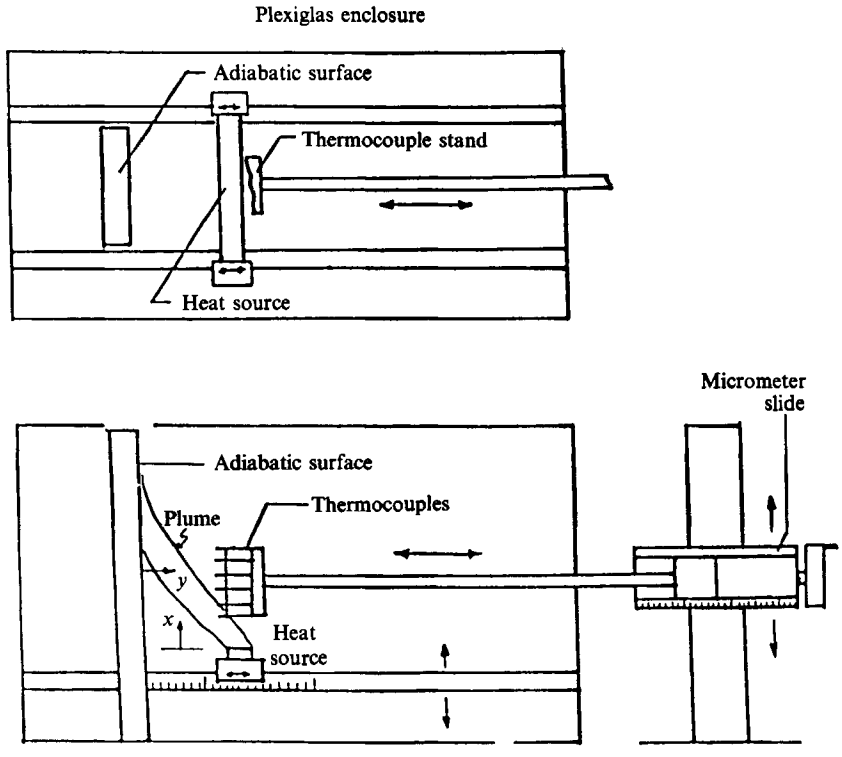

FIGURE 2. Experimental arrangement.

employed to electrically heat the steel strip. The electrical input to the strip could be varied from 0 to around 40 W/m, and was determined by measuring the current and the voltage across the source using a Hewlett-Packard digital voltmeter. The width of the strip l_1 could also be varied from about 0.005 to 0.03 m.

The temperature measurements in the flow were taken with copper–constantan thermocouples made from wires of 2.54×10^{-4} m diameter. The output signal from the thermocouples was measured by means of a digital voltmeter, which gave an accuracy of around 0.25 °C in the measurement. A thermocouple rack was designed to hold an array of six thermocouples in order to expedite the data acquisition process. The thermocouples could be positioned at any orientation and the stand could be moved across the flow by use of a micrometer slide, which had a least count of 10^{-5} m. The slide was itself mounted on a vertical lead screw slide, as shown in figure 2. Thus, the slide could also be moved in the vertical direction. The least count of the vertical slide was 10^{-3} m. Also, the flow field was visualized by employing the shadowgraph technique. The vertical and horizontal surfaces were unheated masonite boards, insulated at the back, and so approximated the adiabatic conditions in figure 1.

As mentioned above, both the experimental and the numerical efforts were directed at circumstances where a strong interaction arises. The flow is expected to be essentially unaffected by the wall if the source is at a relatively large distance from it. The flow then becomes a freely rising thermal plume, which has been investigated by several researchers, see Jaluria (1980). This flow was found to arise for l_2/l_1 larger than about 5.0. Some measurements were initially taken on the freely rising plume, thus obtained, to confirm the accuracy of our measurements. As the source was

brought closer to the vertical surface, a weak interaction, which was very susceptible to extraneous disturbances, was first found to arise, followed by a much stronger interaction at small values of l_2/l_1. This interaction is studied here and some of the typical results obtained are presented and discussed in the next section. All the results are shown for a Prandtl number value of 0.7, which applies for air at normal room temperatures.

4. Results and discussion

4.1. *Numerical results*

The first aspect considered was the numerical simulation of the natural convection flow generated by a heated, vertical, surface, with a uniform heat flux input. The flow near the leading edge is governed by the full Navier–Stokes equations as given by (14)–(16) because the vertical diffusion terms are not negligible in this region, see Mahajan & Gebhart (1978). Far downstream, these diffusion terms become negligible compared with the transverse diffusion terms, and the boundary-layer approximations may be made. Thus, this problem is quite similar to the flow being considered in the present work and is employed to test the numerical scheme. Figure 3(*a*) shows the computed velocity profiles, along with those from the similarity analysis of Sparrow & Gregg (1956). More recent work on this flow is reviewed by Gebhart *et al.* (1988). Clearly, the numerical results are close to those obtained by similarity analysis. Figure 3(*b*) shows a comparison between the two in terms of the downstream surface temperature variation. The computed results deviate from the similarity analysis, which is based on the boundary-layer equations, at small values of X, becoming almost identical to the similarity results at large X. This figure, therefore, indicates the decay of non-boundary-layer or leading-edge effects as the flow proceeds downstream. The results shown in figure 3 also lend strong support to the numerical scheme being employed here.

The study then considered a finite-size heat source on a horizontal adiabatic surface. The vertical wall was also taken as adiabatic. The parameters l_2/l_1 and the Grashof number were taken at typical values of 1 and 10^4, respectively. The time-dependent solution was computed till the steady-state was attained at large time.

The lines of constant Ψ, obtained from the numerical solution for the flow, are shown in figure 4(*a*). The ambient fluid far from the vertical surface enters the region horizontally at the ambient temperature, as expected from the imposed boundary conditions, and arises adjacent to the surface owing to the thermal buoyancy imparted by the heat input. There is also a small recirculation region set up in the corner due to the shearing action of the main flow. The streamlines are seen to dip downward near the source before rising. This is the consequence of large pressure gradients that arise near the source owing to buoyancy effects and has been well documented for flow near the leading edge, see Gebhart *et al.* (1988). Figure 4(*b*) shows the corresponding isotherms. The local temperature and the temperature gradient are highest near the source, as expected, and, therefore, the isotherms are spaced very closely in this region. The location of the local maximum temperature is seen to shift sharply toward the vertical wall, indicating a strong interaction of the wake with the surface.

Figure 5 shows the computed velocity and temperature profiles at various downstream locations. The locations of the maximum vertical velocity and temperature are seen to shift toward the vertical plate just downstream of the leading edge, indicating a strong deflection of the plume toward the vertical wall as

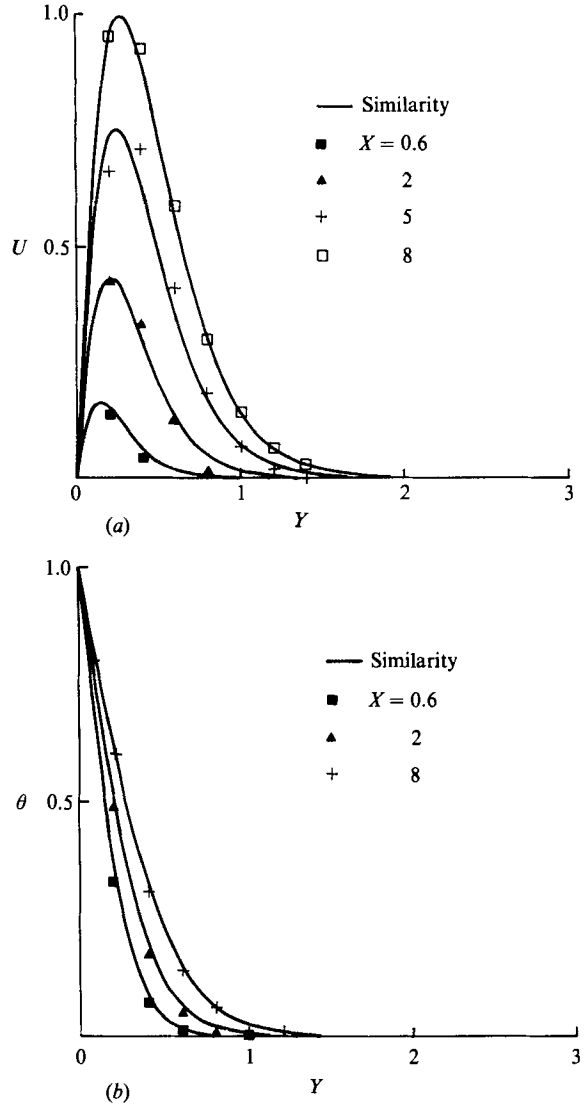

FIGURE 3. Comparison of (*a*) the computed velocity profiles and (*b*) the surface temperature distribution for a vertical, uniform-heat-flux surface at $Gr = 10^4$ with the similarity solution.

sketched in figure 1. Far downstream ($X \geqslant 5$), the location of the maximum velocity is seen to move very gradually away from the wall, indicating that the deflection effects are over and that the flow is similar to a wall plume generated by an upstream heat source. Such a wall plume continues to entrain ambient fluid and to thicken downstream, resulting in a slight outward shift of the location of the maximum vertical velocity, see Jaluria & Gebhart (1977).

Once the numerical solution to the governing equations is obtained in terms of the vorticity and the stream function, the pressure distribution can be determined by solving the Poisson equation for the pressure, given by

$$\nabla^2 P = 2\left[\left(\frac{\partial^2 \Psi}{\partial X^2}\right)\left(\frac{\partial^2 \Psi}{\partial Y^2}\right) - \left(\frac{\partial^2 \Psi}{\partial X \partial Y}\right)^2\right] + \frac{\partial \theta}{\partial X}. \tag{21}$$

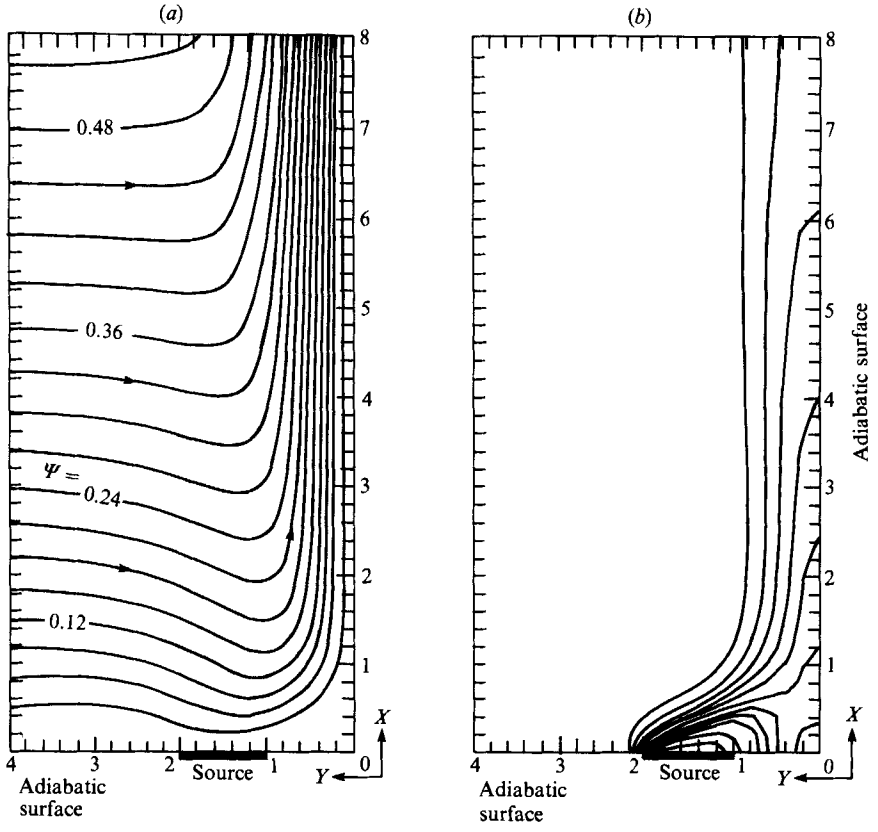

FIGURE 4. Plot of (*a*) streamlines and (*b*) isotherms at $l_2/l_1 = 1$ and $Gr = 10^4$ for adiabatic vertical and horizontal surfaces.

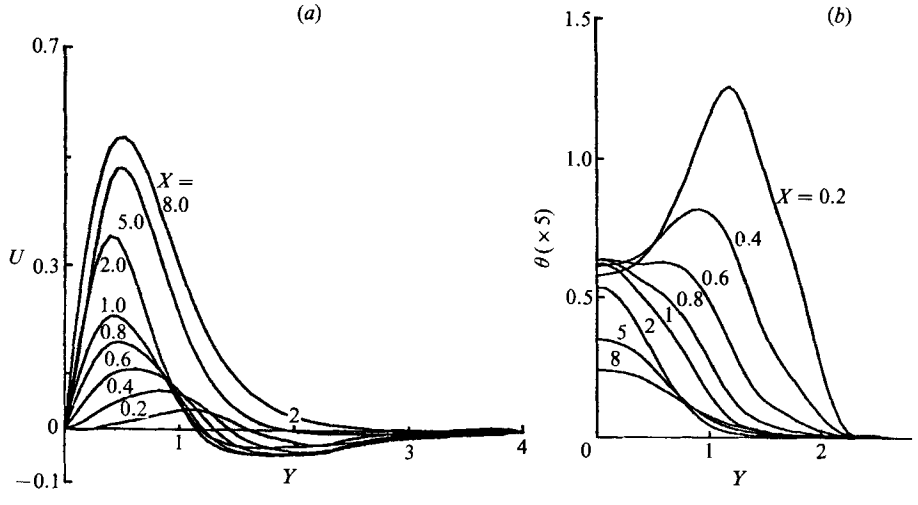

FIGURE 5. Downstream (*a*) velocity and (*b*) temperature profiles at $l_2/l_1 = 1$, $Gr = 10^4$, for adiabatic vertical and horizontal surfaces.

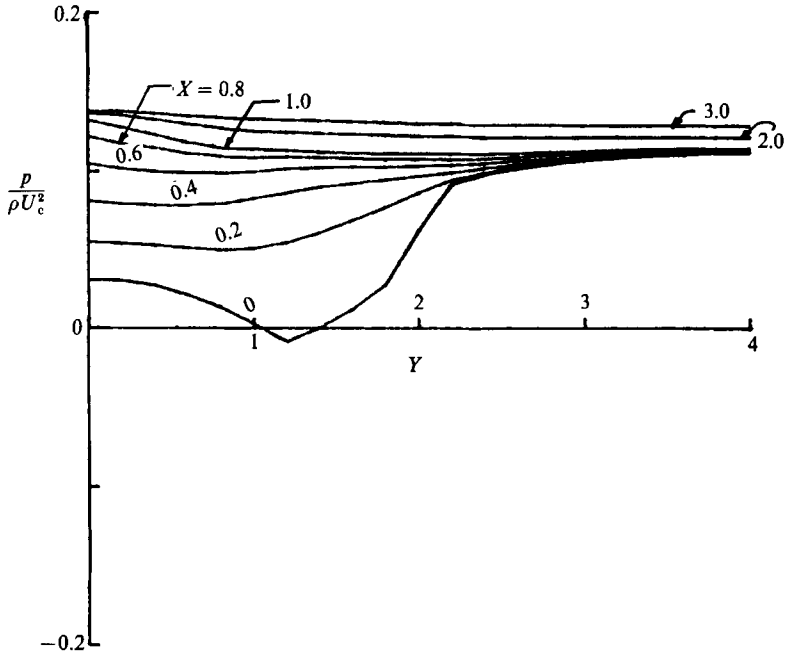

FIGURE 6. Downstream pressure variation at $l_2/l_1 = 1$ and $Gr = 10^4$, for the flow configuration of figure 4.

Details on the derivation of this equation and the numerical procedure for solving it are given by Roache (1976). The successive over-relaxation (SOR) method was employed here for solving this equation from the computed Ψ-distribution. The corresponding boundary conditions on p are obtained from (2) and (3), see Roache (1976). Figure 6 shows the pressure distribution at various downstream locations, with the pressure p being non-dimensionalized by ρU_c^2. There is a significant difference between the ambient pressure and the pressure in the flow near the leading edge. This pressure difference is the driving mechanism for the entrainment of the ambient fluid into the flow. It must be noted that the pressure p here is the motion pressure. The hydrostatic pressure term has been combined with the body force term to yield the buoyancy effect, see Jaluria (1980). The hydrostatic pressure due to the gravitational field obviously decreases with height. However, the motion pressure which arises owing to the flow is seen to increase. This latter effect is due to the decrease in the entrainment velocity with X (Jaluria 1980). A difference in pressure between the inner and outer regions of the flow is seen to arise. This pressure difference exerts a horizontal force on the flow and causes it to deflect toward the vertical surface. As the flow proceeds downstream, the pressure field becomes almost homogeneous. This indicates that the plume becomes attached to the wall and starts developing like a boundary-layer flow.

It is expected that, far downstream, the flow characteristics would approach those of a wall plume, asymptotically, because of the leading-edge effects decaying downstream. Thus, the flow is expected to behave as if the source were a concentrated line heat source located at the leading edge of the vertical plate. Therefore, the solution at large X was compared with the solution of a wall plume arising from a line heat source located at the leading edge of a vertical surface. This solution has been obtained by Jaluria & Gebhart (1977), using similarity analysis. It

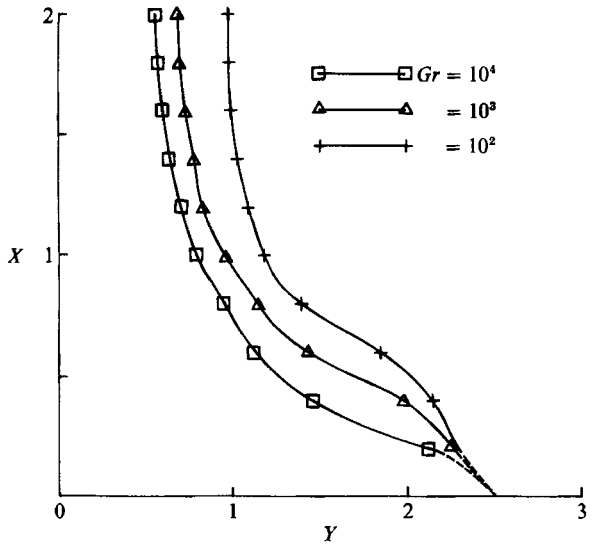

FIGURE 7. Numerically predicted velocity centrelines for various values of the Grashof number Gr at $l_2/l_1 = 2$, for the flow configuration of figure 4.

was found that the solution does approach the wall plume characteristics downstream, in terms of surface temperature decay and maximum vertical velocity increase. The former varies as $Q^{\frac{4}{5}}x^{-\frac{3}{5}}$ and the latter as $Q^{\frac{2}{5}}x^{\frac{1}{5}}$, where $Q = ql_1$ is the total heat input per unit transverse dimension, see Jaluria (1980). Thus, at large x, the flow is found to asymptotically approach these variations, though these trends are not shown here for brevity.

The main dimensionless parameters in the problem are the Grashof number Gr and the geometry ratio l_2/l_1, which were also varied. The effect of the Grashof number is best shown in terms of the flow centreline, which is a plot of the location of the local maximum vertical velocity component in the flow on an (X, Y)-plane. Figure 7 shows the velocity centrelines obtained for $Gr = 10^2$, 10^3 and 10^4. The parameter l_2/l_1 was kept at 2 for all the three cases. The flow centrelines are seen to be deflected toward the vertical wall, indicating a strong interaction between the plume and the wall. As the Grashof number Gr is increased, the deflection of the centreline increases, indicating a stronger interaction at higher Gr. The flow becomes more vigorous as Gr is increased, for a given value of l_2/l_1. This is expected to lead to a larger pressure imbalance and, hence, a stronger interaction.

The effect of varying the ratio l_2/l_1 is shown in figure 8 in terms of the vertical surface temperature variation for two values of this ratio. The Grashof number Gr was taken as 10^4 for both the cases. For convenience and for showing the difference in the temperature levels, the non-dimensional results, in terms of θ, were converted into the physical temperature difference, $T_0 - T_a$, assuming a source width of 1 cm. This plot shows an initial increase in the surface temperature as X increases, followed by a decay. This trend is expected, since the merging of the flow with the surface will cause the surface to heat up. The observed decay is due to the entrainment of ambient fluid into the flow, as the flow moves downstream. For the higher value of the ratio, the location of the peak temperature is seen to be at a larger X value. This suggests a delayed merging of the plume with the vertical surface or, in other words, a weaker interaction. Thus, as l_2/l_1 is increased, the interaction grows weaker till at

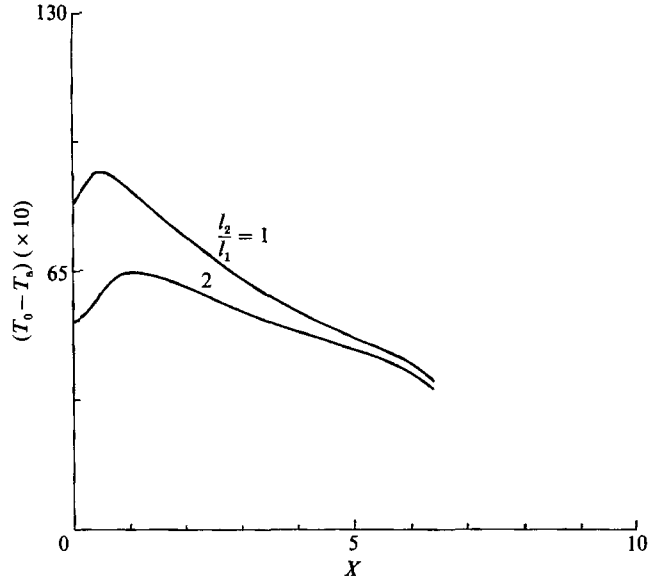

FIGURE 8. Variation of the surface temperature excess, $T_0 - T_a$, with height at $l_2/l_1 = 1$ and 2, for $Gr = 10^4$ and adiabatic vertical and bottom surfaces.

$l_2/l_1 \gtrsim 5$, the interaction was found to be negligible and the plume to rise vertically without deflection.

The effect of varying the boundary conditions at the leading edge was considered next. First the horizontal plate at the leading edge was assumed to be isothermal and at the ambient temperature (Case 2*a*). Then, the vertical surface was also assumed to be isothermal (Case 2*b*). The general nature of the interaction was found to be similar to that given above. However, the interaction was found to be less severe in these cases, as shown in figure 9. This is expected because the flow loses energy owing to conduction at the isothermal boundaries. Thus, the actual energy imparted to the flow is smaller in these cases.

Next, an extensive medium was assumed to exist below the leading edge and entrainment from below was allowed. The boundary conditions applied at the leading edge and the streamline pattern obtained are shown in figure 10. The values of Gr and l_2/l_1 were taken as 10^4 and 1, respectively. The downstream flow indicates the expected larger flow rate, as compared to that for figure 4. A strong entrainment is found to arise from below, between the heat source and the wall. But there is essentially no entrainment from below at the other end of the source. However, the boundary conditions employed here do not perfectly approximate the frequently encountered practical situations. The problem with this particular case lies with the imposition of the velocity boundary conditions at the leading edge of the vertical surface. Only vertical flow is allowed at the leading edge of the vertical plate. The actual situation which needs to be solved is given by (11) and (12). However, this is a much more difficult problem to solve numerically because of the existence of an isolated no-slip surface in the computational domain. Thus, the results shown in figure 10, though not very accurate near $X = 0$, do represent the downstream flow quite satisfactorily. More detailed work on such open boundaries has been carried out by Abib & Jaluria (1988), who have shown that, except for the region very close to the opening, the flow is satisfactorily simulated by imposing suitable boundary conditions at the opening.

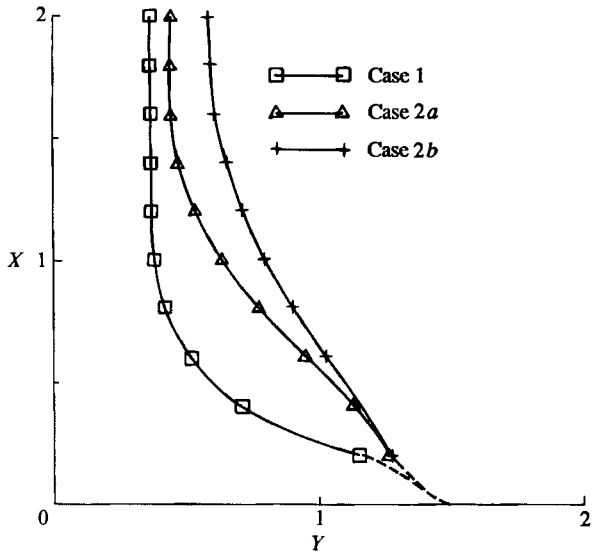

FIGURE 9. Computed velocity centrelines for $l_2/l_1 = 1$ and $Gr = 10^4$. (*a*) adiabatic vertical wall and bottom (Case 1); (*b*) adiabatic vertical wall and isothermal bottom at $\theta = 0$ (Case 2*a*); (*c*) both vertical wall and bottom plate isothermal at $\theta = 0$ (Case 2*b*).

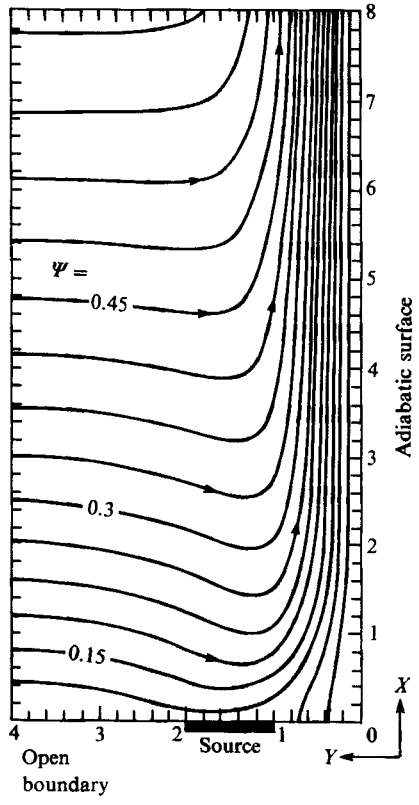

FIGURE 10. Streamlines for the flow that results when the vertical wall is adiabatic and entrainment is allowed from below at $l_2/l_1 = 1$ and $Gr = 10^4$.

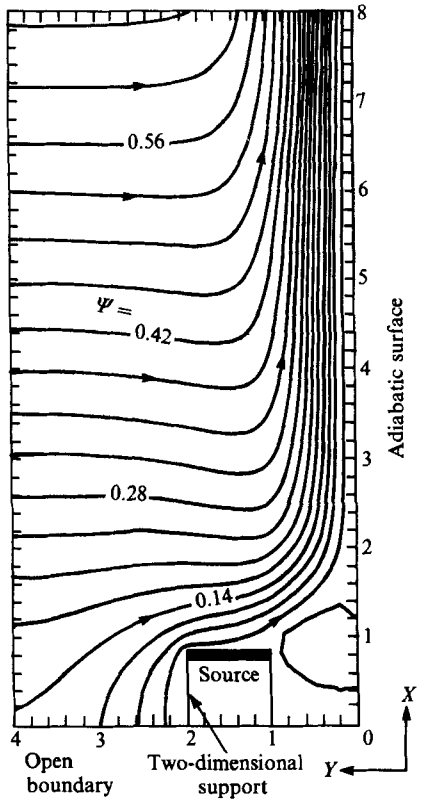

FIGURE 11. Streamlines for the flow resulting from a source located on a two-dimensional support, with the vertical wall adiabatic and entrainment allowed from below, at $l_2/l_1 = 1$ and $Gr = 10^4$.

An important practical circumstance is one in which the heat source is located on a two-dimensional support, with an extensive ambient medium below. Entrainment is allowed from below. The boundary conditions imposed and the flow pattern obtained are shown in figure 11, in terms of streamlines. There is a circulation set up between the vertical wall and the two-dimensional support, on which the source is located. Owing to the no-slip conditions at the source support and at the wall, very little entrainment arises from below between these two. However, a substantial entrainment arises on the other side of the source. The interaction in the above two cases was found to be less severe than the configurations in which entrainment was not allowed from below. This agrees with the experimental results of Pera & Gebhart (1976).

These numerical results indicate the importance of geometry in determining the intensity of the flow interaction. The thermal conditions at the boundaries are also important since these affect the energy entering the flow. The resulting flow and thermal fields in the various configurations considered thus indicate the nature and characteristics of the flow deflection toward the surface. Several other values of the governing parameters were also considered and the basic trends were found to be similar to those discussed above.

4.2. *Experimental results*

The objective of the experimental study was to obtain qualitative and quantitative information on the physical nature of the interaction and to compare the trends thus obtained with those predicted numerically. Qualitative results were obtained mainly through visualization of the temperature field above the heat source, employing the shadowgraph technique. The source width was taken as 0.018 m for the results shown in figure 12. Figures 12(*a*) and (*b*) show the shadowgraphs for two different heat inputs, 10 W/m and 20 W/m, respectively. The corresponding Grashof numbers are 3×10^4 and 6×10^4, respectively, based on the source width l_1. Both the shadowgraphs show an inward deflection of the temperature field, indicating a strong interaction. Figure 12(*b*) also shows that the interaction grows stronger as the Grashof number is increased. This agrees with the numerical predictions, see figure 7. Figure 12(*c*) shows the thermal field for a Grashof number of 3×10^4 when the entrainment coming from below is restricted by placing a plate below the source. As expected and, as predicted numerically, the interaction was seen to become much stronger owing to this restriction on the entrainment. In all the cases shown, the ratio l_2/l_1 was kept at 1. Other values of the heat input Q, source width l_1, and separation distance l_2 were also considered. Similar trends to those shown in figure 12 were observed. The trajectory of the plume was also found to agree qualitatively with numerical results, see figure 7.

The temperature profiles in the flow were also measured. The heat input Q was adjusted for the temperature profile measurements in order to compare the experimental data with the numerical results. For the results shown in figures 13–15, the source width was taken as 1 cm and the spanwise dimension was kept at 20 cm, to ensure the two-dimensionality of the flow. Entrainment from below was restricted. Heat was turned on for about 20 min before taking any measurements, in order to allow the system to reach steady-state conditions and as confirmed by surface temperature measurements. The vertical and horizontal plates were masonite boards, which were well insulated on the side away from the interaction region. Thus, the experimental arrangement simulates adiabatic surfaces. This was also confirmed experimentally by measuring the temperature distributions. However, it must be noted that some energy loss, estimated as 10–15% of the input energy, does occur because of conduction into the plates. It is extremely hard to obtain a perfectly insulated surface in air because of the low thermal conductivity of air, which makes it comparable in insulation properties to the plates. Because of this conduction loss, the thermal energy in the flow is reduced, making the flow less vigorous.

The results are presented in terms of the experimentally obtained temperature centreline in figure 13. The plot also shows the corresponding numerically obtained temperature centreline for an adiabatic vertical surface near the source. An initially sharp inward shift of the plume is indicated, followed by a gradual turning of the flow, with the plume eventually merging with the vertical surface. Owing to the adiabatic condition at the surface, the measured local maximum temperature occurs at the wall after the flow merges with the wall, resulting in a wall plume. However, the experimental results indicate a somewhat weaker interaction, as compared to the analytical results. This is expected from the reduction in thermal energy in the flow due to energy loss to the surface in the experiment. Results were also obtained for the case when entrainment from below was allowed. As predicted by the numerical study, the interaction was found to be much weaker in this case, as compared to that

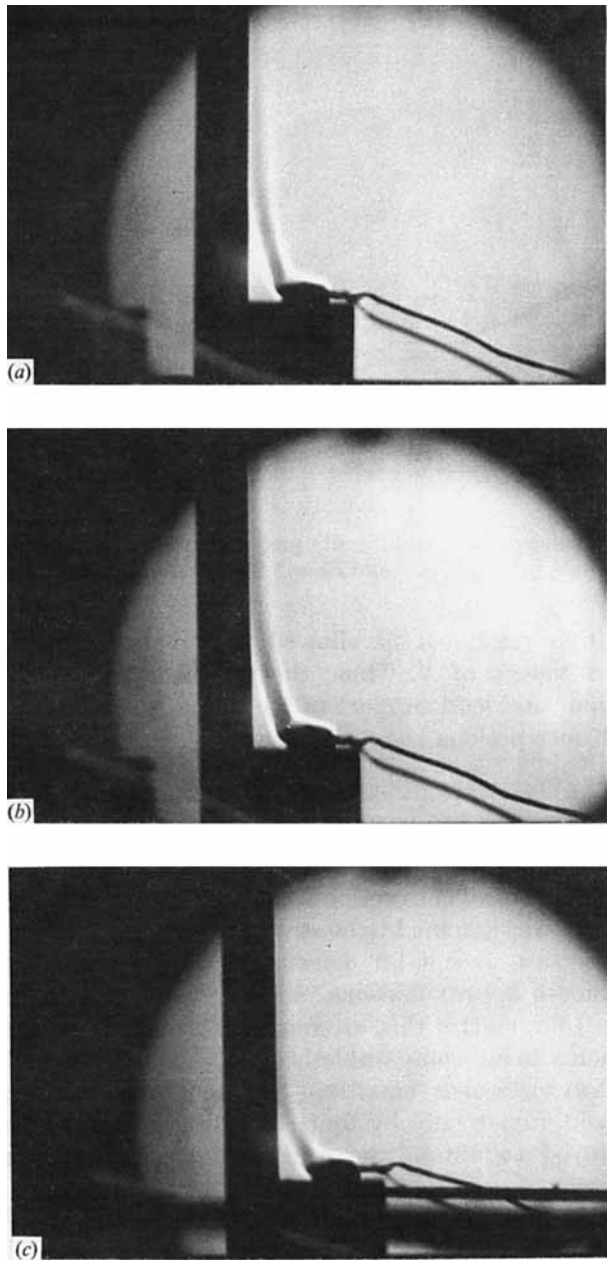

FIGURE 12. Shadowgraphs of the thermal field at $l_2/l_1 = 1$ and (*a*) $Gr = 3 \times 10^4$, with entrainment allowed from below; (*b*) $Gr = 6 \times 10^4$, with entrainment allowed from below; (*c*) $Gr = 3 \times 10^4$, with entrainment restricted from below.

seen in figure 13, due to the induced entrainment from below which reduces the pressure imbalance. These aspects were considered in detail earlier.

The temperature profiles were also measured and these indicated a fairly good agreement with the numerical results, when the actual energy entering the flow was estimated and employed in the normalization, as shown in figure 14, for the two cases

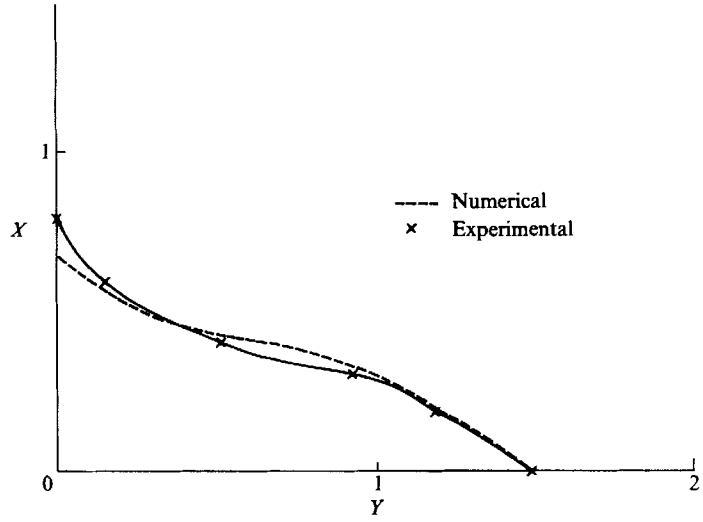

FIGURE 13. Comparison of the numerically predicted and the experimentally obtained temperature centrelines at $l_2/l_1 = 1$ and $Gr = 1.8 \times 10^4$ for the configuration of figure 4.

of entrainment either restricted or allowed from below. Similar agreement was observed for other values of X. Thus, the experimental results agree with the numerical predictions and lend support to the numerical simulation, which may be employed for such interactions between natural convection wakes and surfaces in close proximity.

5. Conclusions

The interaction of a natural convection wake with a vertical unheated surface was investigated. The flow was assumed to be steady, two-dimensional, laminar and with constant fluid properties, except for density variations which were considered in terms of the Boussinesq approximations. A numerical and experimental study has been conducted to characterize this interaction. The problem is elliptic in nature owing to the gradients being comparable in both the directions. Therefore, the full two-dimensional Navier–Stokes equations in the vorticity–stream function formulation were solved numerically by finite-difference methods. The false transient method was employed to obtain the solution, using the Alternating Direction Implicit (ADI) scheme.

The interaction was studied mainly in terms of the deflection of the flow toward the surface. Over the range of the physical variables considered particularly the Grashof number Gr and the geometry ratio l_2/l_1, the temperature and velocity centrelines were found to be deflected sharply towards the surface, immediately downstream of the heat source. Increasing the heat input increased the deflection, while moving the source away from the vertical surface reduced it. The boundary conditions at the leading edge were found to affect the flow significantly. A restriction imposed on the entrainment entering from below resulted in a more severe interaction as shown by the deflection of the flow. The computed pressure field showed an imbalance across the plume, indicating the cause for the deflection toward the surface. The interaction was found to become weaker when the horizontal and vertical surfaces were taken as isothermal at the ambient temperature, owing to the

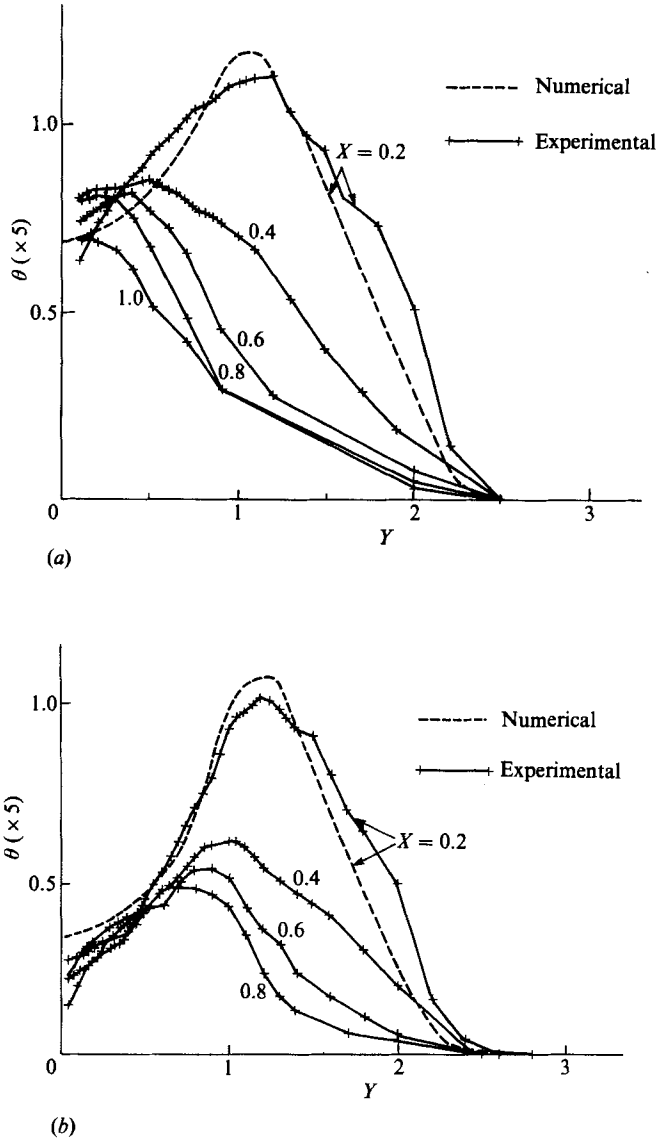

FIGURE 14. Measured temperature profiles at various downstream locations for $l_2/l_1 = 1$ and $Gr = 1.8 \times 10^4$: (*a*) the configuration of figure 4, with no entrainment from below the source; (*b*) entrainment allowed from below the source.

energy loss to the surfaces. Finally, the experimental and numerical results showed fairly good agreement, lending support to the numerical model employed and to the predictions obtained.

The authors acknowledge the financial support provided by the National Science Foundation, under Grant Nos. MEA-82-14325 and CBT-84-15364 for this work.

REFERENCES

ABIB, A. & JALURIA, Y. 1988 Numerical simulation of the buoyancy-induced flow in a partially open enclosure. *Num. Heat Transfer* **14**, 235–254.

BOURQUES, C. & NEWMAN, B. G. 1980 Reattachment of a two-dimensional incompressible jet to an adjacent flat plate. *Aero. Quart.* **11**, 201–210.

CHAN, Y. L. & TIEN, C. L. 1985 A numerical study of two-dimensional laminar natural convection in shallow open cavities. *Intl J. Heat Mass Transfer* **28**, 603–612.

GEBHART, B., JALURIA, Y., MAHAJAN, R. L. & SAMMAKIA, B. 1988 *Buoyancy Induced Flows and Transport.* Hemisphere.

GEBHART, B., SHAUKATULLAH, H. & PERA, L. 1976 The interaction of unequal laminar plane plumes. *Intl J. Heat Transfer* **19**, 751–756.

GRELLA, J. J. & FAETH, G. M. 1975 Measurements in a two-dimensional thermal plume along a vertical adiabatic wall. *J. Fluid Mech.* **71**, 701–710.

HARDWICK, N. E. & LEVY, E. K. 1973 Study of the laminar free convection wake above an isothermal vertical plate. *Trans. ASME* C: *J. Heat Transfer* **95**, 289–294.

JALURIA, Y. 1980 *Natural Convection Heat and Mass Transfer.* Pergamon.

JALURIA, Y. 1982 Thermal plume interaction with vertical surfaces. *Lett. Heat Mass Transfer* **9**, 107–117.

JALURIA, Y. 1985*a* Natural convective cooling of electronic equipment. In *Natural Convection: Fundamentals and Applications* (ed. S. Kakac, W. Aung & R. Viskanta). Hemisphere.

JALURIA, Y. 1985*b* Interaction of natural convection wakes arising from thermal sources on a vertical surface. *Trans. ASME* C: *J. Heat Transfer* **107**, 883–892.

JALURIA, Y. & AGARWAL, R. 1986 Computational study of nonboundary layer external natural convection flows. *Proc. Intl Conf. Comput. Mech., Tokyo*, vol. VIII, pp. 189–194. Springer.

JALURIA, Y. & GEBHART, B. 1977 Buoyancy-induced flow arising from a line thermal source on an adiabatic vertical surface. *Intl J. Heat Mass Transfer* **20**, 153–157.

JALURIA, Y. & TORRANCE, K. E. 1986 *Computational Heat Transfer.* Hemisphere.

LIEBERMAN, J. & GEBHART, B. 1969 Interactions in natural convection from an array of heated elements. *Intl J. Heat Mass Transfer* **12**, 1385–1396.

MAHAJAN, R. L. & GEBHART, B. 1978 Higher order approximations of the natural convection flow over a uniform flux vertical surface. *Intl J. Heat Mass Transfer* **21**, 549–556.

MALLINSON, G. D. & DE VAHL DAVIS, G. 1975 The method of the false transient for the solution of coupled elliptic equations. *J. Comp. Phys.* **12**, 435–461.

MILLER, D. R. & COMINGS, E. W. 1960 Force-momentum fields in a dual jet flow. *J. Fluid Mech.* **7**, 237–256.

PEACEMAN, D. & RACHFORD, H. 1955 The numerical solution of parabolic and elliptic differential equations. *J. Soc. Indust. Appl. Maths* **3**, 28–41.

PERA, L. & GEBHART, B. 1976 Laminar plume interactions. *J. Fluid Mech.* **68**, 259–271.

QUINTIERE, J. 1984 A perspective on compartment fire growth. *Combust. Sci. Tech.* **39**, 11–54.

REBA, I. 1966 Application of the Coanda effect. *Sci. Am.* **21**, 84–92.

ROACHE, P. J. 1976 *Computational Fluid Dynamics.* Albuquerque: Hermosa.

SAWYER, R. A. 1963 Two-dimensional reattaching jet flows including the effects of curvature on entrainment. *J. Fluid Mech.* **17**, 481–497.

SPARROW, E. M. & GREGG, J. L. 1956 Laminar free convection from a vertical plate with uniform surface heat flux. *Trans. ASME* C: *J. Heat Transfer* **78**, 435–440.

YANG, K. T. & JERGER, E. W. 1964 First-order perturbations of laminar free convection boundary layers on a vertical plate. *Trans. ASME* C: *J. Heat Transfer* **86**, 107–115.